

Inhibitory Postsynaptic Potentials

Carry Synchronized Frequency

Information in Active Cortical Networks

Andrea Hasenstaub, Yousheng Shu,
Bilal Haider, Udo Kraushaar,
Alvaro Duque, and David A. McCormick

Supplemental Experimental Procedures

Mathematical Methods

Power spectra, transfer functions, and auto- and cross-correlograms were computed in MATLAB 7.0.1 (The MathWorks, www.mathworks.com). Power spectra were calculated using Welch's method. All correlations were normalized so that autocorrelations would be 1 at zero lag. Shufflegrams were computed by correlating each UP state segment with a randomly selected UP state segment in either the same cell (auto-correlograms) or the second cell (cross-correlograms), without replacement. Continuous transfer functions were estimated using Welch's averaged periodogram method. Discrete transfer functions were estimated using Wiener's method. For calculation of power spectra and correlations during UP states, 200-300 millisecond periods of network activity were selected randomly by the computer program; the spectrum or correlation was calculated for each period, and the correlations or spectra were averaged together to get the estimated correlation or spectrum for each cell. All error bars were calculated as the standard error of the mean.

To measure gamma modulation of synaptic barrage or spike rate, the extracellular recording was band-pass filtered at 30-80 Hz. Large troughs (at least half as large as the largest troughs present) in the resulting waveform were identified in Spike2, and trough-triggered averages of the gamma-band extracellular recording, extracellularly recorded spike rate (for figure 5), and intracellularly recorded membrane potential (for figure 6), were constructed. The dominant frequency in the gamma band varied from day to day, so to combine trough-triggered averages from different recordings, the time of the peak in the trough-triggered gamma-band average immediately following the central trough was taken to be half the dominant frequency; the time axes gamma average and spike or membrane potential average were both normalized so that the time of the gamma trough was 0 (cycles) and the time of the gamma peak was 0.5 (half a cycle).

A number of experiments were performed with a dynamic clamp technique using a DAP-5216a board (Microstar Laboratory) (Dorval, 2001). Noisy conductances were constructed according to an Ornstein-Uhlenbeck (colored noise) model (Destexhe et al., 2001). For measurement of subthreshold transfer function, a cell was placed at its resting potential; a conductance with reversal potential of 0 mV, a time constant of 5 ms, and whose standard deviation was half its mean, was injected into the cell. The standard deviation (and, concurrently, the amplitude) of the conductance was adjusted to give a 10 mV peak-to-peak membrane potential deviation, and the holding current was adjusted to keep the cell just below spike threshold. Transfer function from the injected conductance to the recorded membrane potential fluctuations was then calculated. For measurement of suprathreshold transfer function, the cell was then depolarized to give a mean spike rate of 5 Hz, and the transfer between the injected conductance and the spike times was calculated. For mimicking natural recurrent activity, two dynamic clamp systems were used in parallel: one generated a conductance with a reversal potential of 0 mV (mimicking excitation) and the other generated a conductance with a reversal potential of -80 mV (mimicking inhibition). Inhibitory and excitatory conductance patterns were constructed, starting from naturally occurring (DC-removed) IPSP and EPSP barrages *in vivo*: 20-second long sequences of model IPSPs and EPSPs with power spectra that matched the average power spectra of IPSP and EPSP barrages in n=12 pyramidal neurons were constructed, the model PSP barrages were converted into currents by RC-correction with resistance and capacitance typical for pyramidal neurons (thus producing a current sequence that, when injected into a cell with the same resistance and capacitance, would produce the same pattern of membrane potential deviations), and the injected conductances were taken to be proportional to the calculated currents. Quality of fit is presented in Supplement 5.

References

- Csicsvari, J., Hirase, H., Czurko, A., Mamiya, A., and Buzsaki, G. (1999). Oscillatory coupling of hippocampal pyramidal cells and interneurons in the behaving Rat. *J Neurosci* *19*, 274-287.
- Destexhe, A., Rudolph, M., Fellous, J. M., and Sejnowski, T. J. (2001). Fluctuating synaptic conductances recreate in vivo-like activity in neocortical neurons. *Neuroscience* *107*, 13-24.
- Dorval, A. D., Christini, D.J., White, J.A. (2001). Real-time linux dynamic clamp: A fast and flexible way to construct virtual ion channels in living cells. *Ann Biomed Eng* *29*, 897-907.
- Fellous, J. M., Houweling, A. R., Modi, R. H., Rao, R. P., Tiesinga, P. H., and Sejnowski, T. J. (2001). Frequency dependence of spike timing reliability in cortical pyramidal cells and interneurons. *J Neurophysiol* *85*, 1782-1787.
- McCormick, D. A., Connors, B. W., Lighthall, J. W., and Prince, D. A. (1985). Comparative electrophysiology of pyramidal and sparsely spiny stellate neurons of the neocortex. *J Neurophysiol* *54*, 782-806.
- Nowak, L. G., Azouz, R., Sanchez-Vives, M. V., Gray, C. M., and McCormick, D. A. (2003). Electrophysiological classes of cat primary visual cortical neurons in vivo as revealed by quantitative analyses. *J Neurophysiol* *89*, 1541-1566.
- Pike, F. G., Goddard, R. S., Suckling, J. M., Ganter, P., Kasthuri, N., and Paulsen, O. (2000). Distinct frequency preferences of different types of rat hippocampal neurones in response to oscillatory input currents. *J Physiol* *529 Pt 1*, 205-213.
- Shu, Y., Hasenstaub, A., Badoual, M., Bal, T., and McCormick, D. A. (2003). Barrages of synaptic activity control the gain and sensitivity of cortical neurons. *J Neurosci* *23*, 10388-10401.

Figure S1. The Spike Refractory Period following an Action Potential in a FS Interneuron Is Shorter than That in a RS Cell

A. Stimulus protocol for examining the amplitude-time course of the spike refractory period. Two 12.5 msec duration half sine wave current stimuli are injected. The first stimulus is either just subthreshold or just suprathreshold for action potential generation. Following this, a second random-amplitude stimulus is injected at a random delay. Shown is the overlay of the full family of injected currents. Protocol from (Shu et al., 2003). B. Raw example of the response of the FS neuron to the protocol in A. C, D. Change in probability of generating a spike (color) as a function of delay between the two stimuli (x-axis) and the amplitude of the second pulse (y-axis). Note that the refractory period in a pyramidal cell is much longer than in a FS neuron. E. Comparison of the duration of the relative refractory period in n=26 pyramidal neurons and n=8 FS interneurons. Data collected from layer 5 neurons in submerged slices with whole-cell patch-clamp recording. Parts A,B from (Shu et al., 2003)

FS cells represent higher frequency oscillations better in their spike output than RS neurons The ability of FS and RS cells to represent different frequencies of input in their spike output was tested with the intracellular injection of sine wave currents, as well as colored noise. Increasing the frequency of the sine wave injection from 2 to 300 Hz resulted in a steady decrease in the probability that each cycle of the sine wave would activate an action potential in cortical RS neurons. However, fast spiking GABAergic neurons were capable of generating an action potential to each phase of the sine wave current even at frequencies of 100-250 Hz (data not shown; see (Fellous et al., 2001; Pike et al., 2000)).

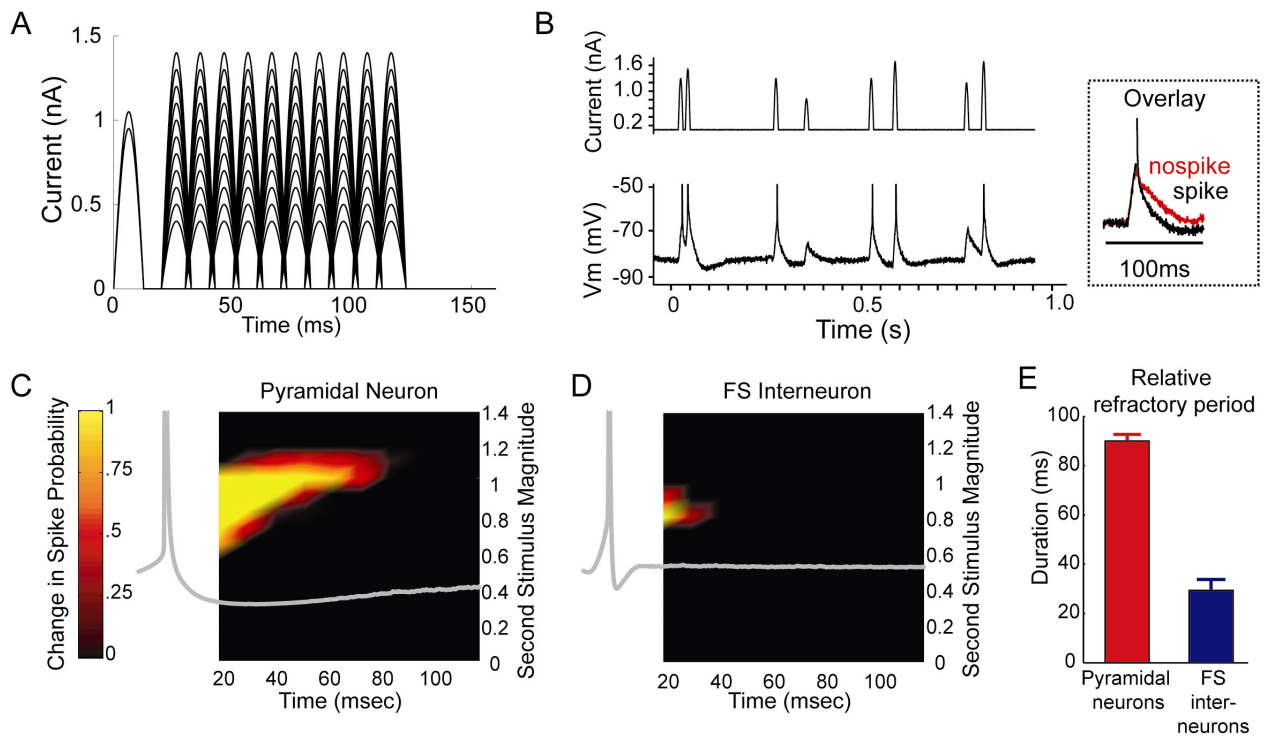


Figure S2. Decrease in Cross-Correlation between EPSP and IPSP Dominated Traces with Increasing Distance between Intracellularly Recorded Cells

IPSP-dominated membrane potentials were recorded near 0 mV and EPSP dominated traces were recorded near -80 mV in ferret prefrontal cortex in vivo during ketamine/xylazine anesthesia (n=6 pairs). Cross correlations were calculated only during the UP state of the slow oscillation, after removal of DOWN state periods as well as transitions between the two states.

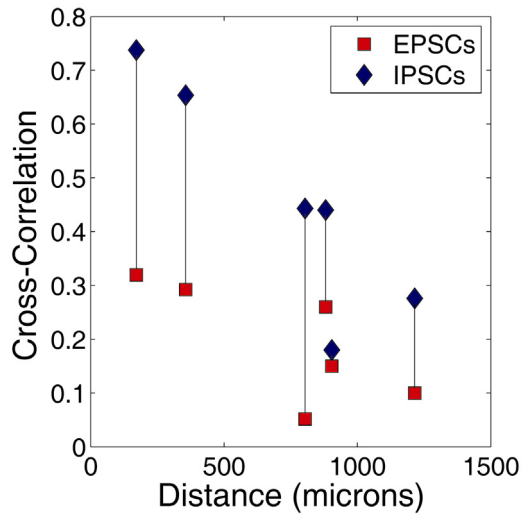


Figure S3. Method for Identification of Fast Spiking (FS) and Regular Spiking (RS) Neurons with Extracellular (A,B) and Whole-Cell or Intracellular (C) Recordings

A,B. Single units were recorded extracellularly with minimal filtering (0.1 – 20,000 Hz). Previous studies have demonstrated that fast-spiking and regular spiking neurons can be accurately separated based upon a combination of two parameters: spike width and the ratio of the positive and negative portions of the waveform (Csicsvari et al., 1999; McCormick et al., 1985). Plotting the measures of these two parameters in the cells recorded clearly revealed two distinct clusters, which we identify as fast spiking and regular spiking neurons. Neurons exhibiting evidence of burst firing in their interspike interval histograms (Nowak et al., 2003) were excluded from analysis. C. Example responses of regular spiking and fast spiking neurons to depolarizing current injection. Note the generation of a high frequency, non-adapting pattern of action potentials in FS neurons. Action potentials are expanded for illustration in the bottom traces. See Nowak et al., 2003, for quantitative criteria for identification of FS and RS neurons.

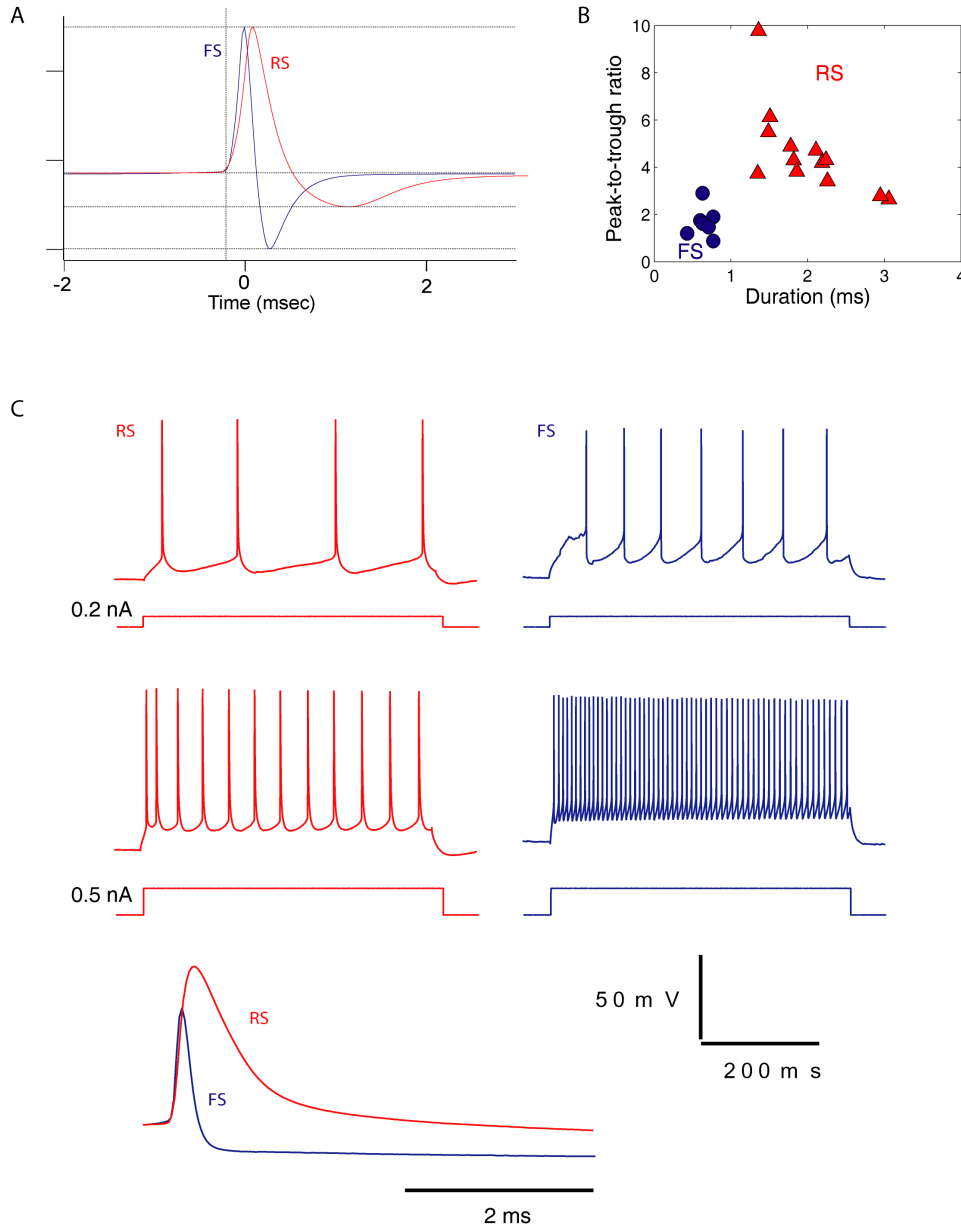


Figure S4. Interspike Interval Histograms of Four Representative RS Cells (Red) and Four Representative FS Cells (Blue) Recorded In Vivo in the Ferret Prefrontal Cortex during the Generation of UP and DOWN States

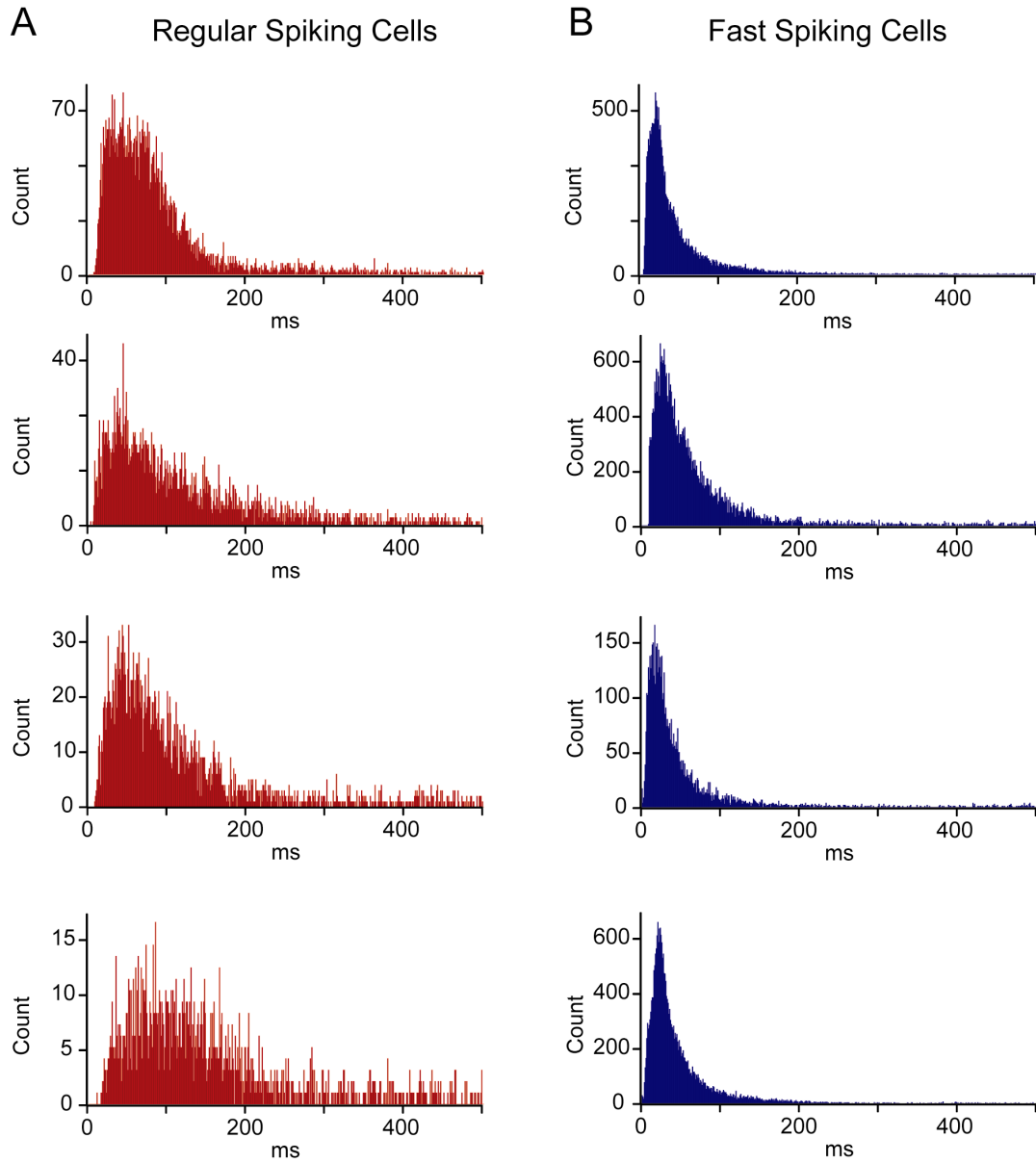


Figure S5. Generation of Naturalistic Excitatory and Inhibitory Conductance Barrages

The (DC-removed) power spectra of multiple 300 ms excerpts of intracellularly recorded synaptic barrages during UP states in regular spiking neurons *in vivo*, when the cell was held near -80 mV (A) and 0 mV (B) in $n=12$ cells, were averaged together to form the typical PSP power spectra (red lines). Model PSPs were constructed by summing an Ornstein-Uhlenbeck component (power spectrum in blue) and a gamma-filtered white noise component (power spectrum shown in orange); the gamma filter characteristics were varied to give the best fit to the observed data. The power spectrum of the combination of the two components (green) closely matches the typical PSP power spectrum. C, D. Power spectra of the model EPSC and IPSC currents following RC correction using resistance and capacitance values typical of those measured *in vitro*. E, F. Dynamic clamp injection of the modeled excitatory currents into a passive RC circuit (the Axon Instruments model cell), using an Axoclamp 2B amplifier in discontinuous current clamp mode, gives output power spectra that generally match the power spectra of the PSPs recorded *in vivo*.

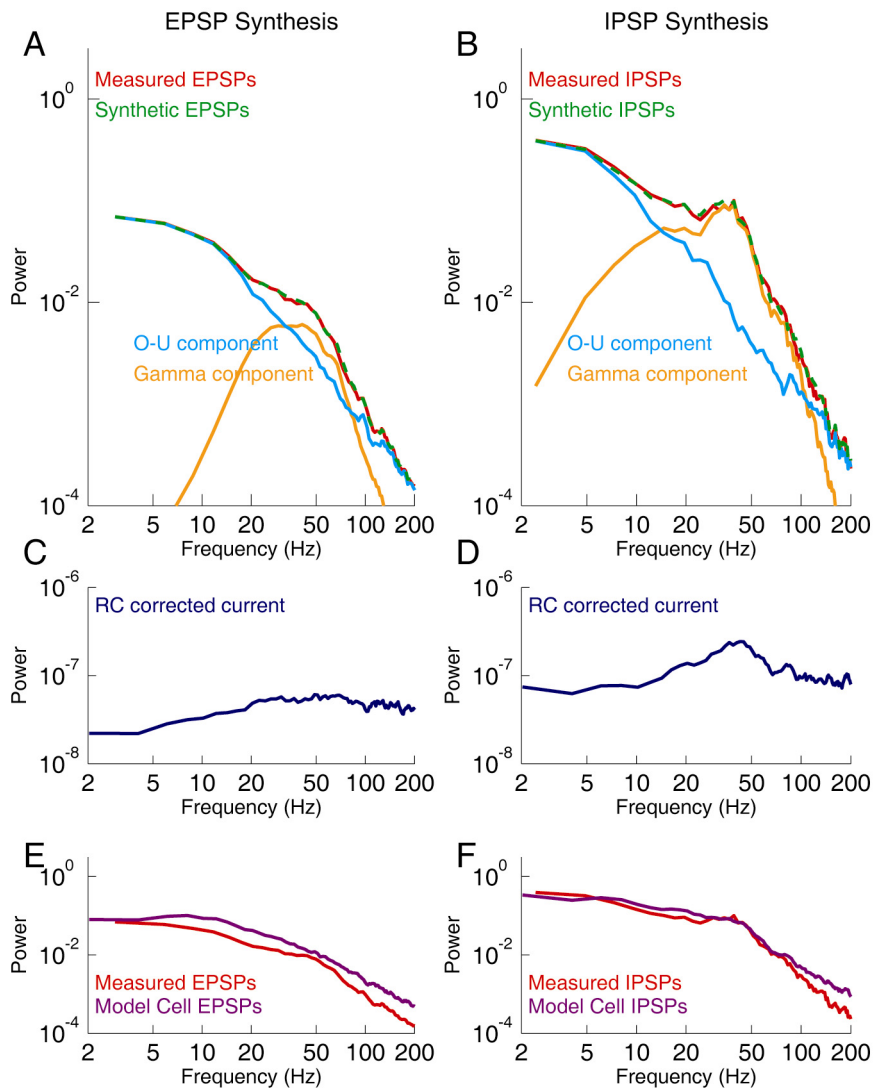


Figure S6. Additional Analysis of the Effects of Inhibitory Conductance on Spike Timing

A. Example of simultaneous injection of excitatory and inhibitory conductance noise into a layer 5 pyramidal neuron. B. The spike-triggered averages of the excitatory and inhibitory conductance noise show that typically, a larger reduction in inhibitory conductance (blue) than increase in excitatory conductance (red) precedes a spike, but the best predictor of a spike is the combination of an increase in excitation and a decrease in inhibition (Green). C. Mean peak or trough height for n=6 cells. D. Cross correlation between the inhibitory conductance and the time of spike initiation (convolved with a 1 msec cosine bell curve). The inhibitory conductance is better correlated with the spike train than is the excitatory conductance; the sum of the excitatory conductance and the negative of the inhibitory conductance is better correlated still. E. Group data for n=6 cells. Bars are standard error.

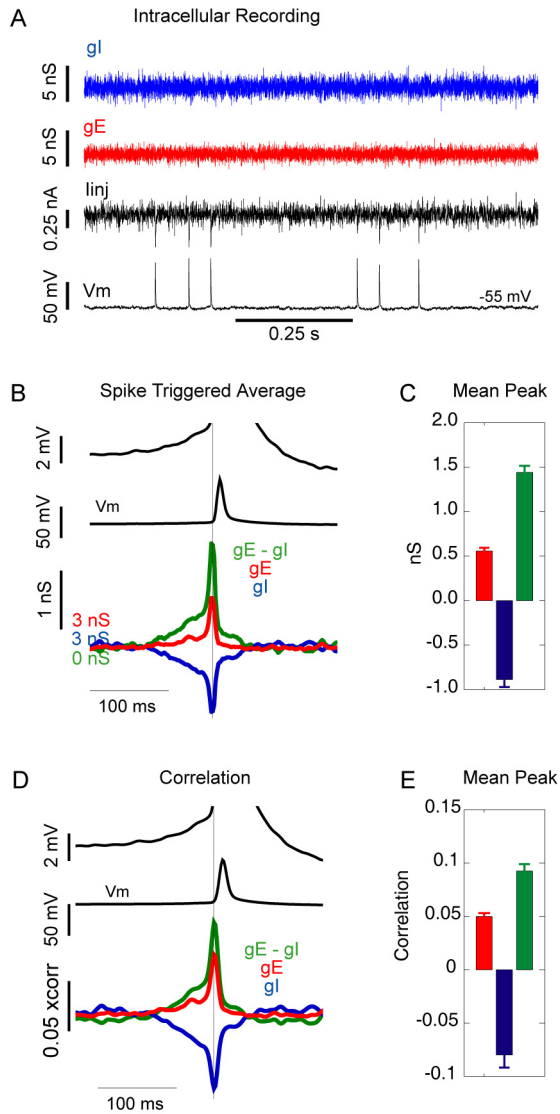
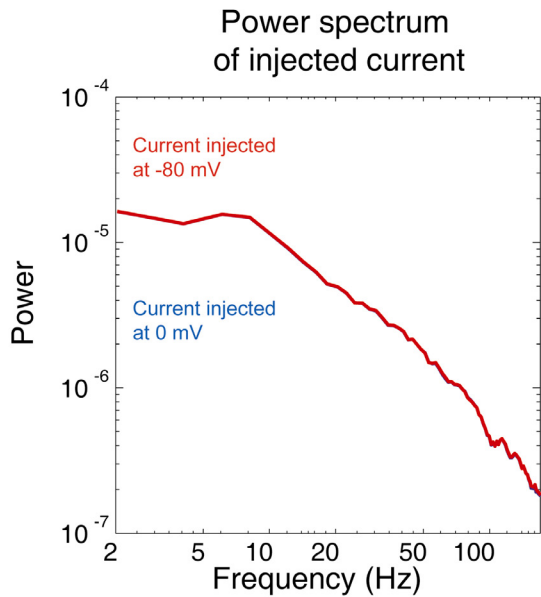


Figure S7. Control Experiment Demonstrating that the Membrane Response of RS Cells to the Injection of Identical Current at 0 mV and -80 mV Is Not Significantly Different at Higher Frequencies

A. Power spectrum of intracellularly injected current noise. The same current was injected simultaneously with DC current to bring the cell's average membrane potential to 0 mV and to -80 mV. B. Power spectrum of membrane response. For frequencies below approximately 20 Hz, the same current noise caused larger membrane potential deflections at -80 mV than at 0 mV, while for higher frequencies the current noise caused equal membrane potential deflections. Nearly identical results were obtained from an additional 5 RS cells in vitro. This result demonstrates that the excess power observed in gamma-band frequencies of PSPs recorded at 0 mV is not simply a result of intrinsic membrane properties.

A



B

